Antenna-Based Popup Vapor Sensor Guided by Controlled Compressive Buckling

Shaghayegh Soltani, *Student Member, IEEE,* Aaron. J. R. Hillier, Simon J. Holder, John C. Batchelor, *Senior Member, IEEE*

Abstract— A novel highly stretchable gas sensor is reported that is based on popup antenna reconfiguration due to the strain induced by the swelling of a polydimethylsiloxane (PDMS) substrate when exposed to diethyl ether. When the swollen substrate is removed from the volatile solvent environment, the PDMS volume increase is reversed leading to compressive stress in an attached antenna transforming a 2D structure to a 3D structure through mechanically induced shaping. This provides a low cost and simple route to tune the antenna resonant frequency and gain in direct response to a chemical stimulus. Our proposed solvent sensor is able to measure 0 to 60% PDMS swelling corresponding to diethyl ether concentrations up to 1620 ppm via a resonant frequency shift from 4 to 2.4 GHz. A fatigue life study indicated $10^{3.5}$ life cycles which demonstrates the durability of these sensors to accommodate large strain and repeatability of the sensing process. Multiphysics Finite Element Method (FEM) modelling of the mechanical and RF simulations along with analytical results based on an equivalent circuit model were in good agreement with experimental data and demonstrate the potential of these structures as sensors.

Index Terms—Compressive stress, popup antenna, diethyl ether, vapor, PDMS, sensor.

I. INTRODUCTION

Chemical vapor environmental exposure can occur from accidental spill during manufacture, distribution, and handling. These gases are often combustive and can threaten public safety [1]. Therefore, designing cost effective low profile wireless sensors capable of monitoring the presence of chemical vapor is of great interest. Diethyl ether is a common laboratory solvent extensively used in chemical and pharmaceutical industries and as an anesthetic for humans in developing countries. Inhalation can irritate the throat and nose, and long-term exposure can cause drowsiness, respiratory issues or even death [2], [3]. It is a volatile chemical that is highly flammable and potentially explosive. Thus, the hazards associated with diethyl ether make monitoring necessary.

To date various attempts have been made to integrate smart materials into antenna designs for wireless gas sensing [4]-[12]. For example, changes to the conductivity of carbon nanotubes or graphene integrated in an antenna, in the presence of chemical vapors led to a shift in resonant frequency [4]-[10]. Furthermore, the variation in optical, electrical and chemical properties of customized nanoparticle dispersion inks with exposure to a particular gas to tune antenna responses have been exploited. For instance, the authors of [11] proposed a gas sensor by embedding an electrode coated with copper acetate-based chemi-resistive ink in a loop antenna, while [12] integrated Tin oxide (SnO_2) nanoparticles into a microstrip patch for detection of ethylene gas. However, the reported materials and fabrication processes can be expensive and complex.

The potential of PDMS (polydimethylsiloxane) swelling in sensing applications is reported in [13]-[21] with antenna properties when embedded in PDMS substrate in [22]-[25]. These studies focused on the substrate flexibility due to its low Young's modulus (less than 2 MPa) at room temperature [26]. However, only a few publications have applied the swelling behavior of PDMS to vapor detection [27], [28]. These designs are spacious and complex, respectively. This paper contributes by combining the swelling properties of PDMS on exposure to chemical vapor with the compressive buckling technique reported in [29]-[35] to introduce a state of the art and robust design for a highly stretchable gas sensor. The elastomeric nature of the substrate allows it to conform to different mounting surfaces [36] and the compressive buckling mechanism transforms the planar antenna design to 3D without complicated fabrication methods. Previous literature has focused on the mechanical aspects of the method and to the authors' knowledge, no research has been reported to use this technique for engineering the antenna performance. This paper is organized as follows, Section II describes the design and simulation procedure. A lumped element model to estimate the antenna resonant frequency is described in Section III. Section IV analyzes the analytical and numerical results. In Section V experimental outcomes are discussed and Section VI concludes the paper.

II. SENSOR DESIGN AND WORKING PRINCIPLE

The proposed vapor sensor mechanism is based on the resonant frequency shift of a half wavelength dipole antenna made of 30 µm thick copper by swelling and deswelling of its elastomeric substrate. The antenna was designed at 2.4 GHz when flat on a double-layer substrate comprising a top layer of thin PDMS and a bottom layer of high permittivity ceramic. In order to achieve a stretchable layout, the dipole is selectively bonded to the fully swollen PDMS substrate. This enables the unbonded sections to

TABLE I
PARAMETERS FOR THE DESIGNED ANTENNA

Parameters	l_1			W_1	l_2	W_2	l_3	W_3	F	T_3
	$T_2=0.4$	$T_2=0.8$	$T_2=1$							
dimensions (mm)	16.31	17.68	18	1	50	18	80	30	3	1

buckle out of plane in response to the induced strain from PDMS swelling and deswelling to avoid fracture. Fig. 1 presents a schematic of the described system including the dipole, PDMS and ceramic substrate. The proposed antenna was designed for 3 different swelling PDMS thicknesses of 0.4 mm, 0.8 mm and 1 mm. All geometrical dimensions and electrical parameters are given in Table I and Table II, respectively. Note that the dimension values in Table I are for PDMS before swelling.

TABLE II
ELECTRICAL PROPERTIES OF THE SUBSTRATES USED IN THE SENSOR DESIGN

Electrical constant	Value
K_{PDMS}	2.55
$Conductivity_{PDMS}$ (S/m)	2×10^{-5}
$K_{Ceramic}$	20
$Conductivity_{Ceramic}$ (S/m)	10^{-11}
$K_{Swollen\ PDMS}$*	2.8±0.04
$Conductivity_{Swollen\ PDMS}$ * (S/m)	0.13±0.004

*At the end of a complete diethyl ether vapor exposure cycle.
K denotes the relative permittivity.

All dielectric properties were measured and averaged in the frequency range of 2.4 GHz to 4 GHz using a SPEAG Dak 3.5 probe with a Rohde and Schwarz ZVL 6 GHz network analyzer using the manufacturer procedure [37].
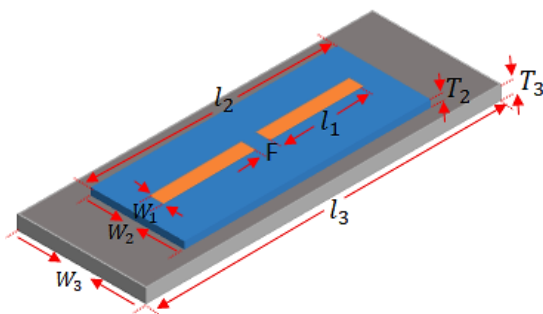

Fig. 1. Geometry of the designed half wavelength dipole antenna.

A modified equivalent circuit model was proposed to describe the popup dipole antenna [38], [39]. This RLC circuit was validated through comparison to multi-physics simulations which were divided into three steps:

1- Electromagnetic simulation to design a planar half wave dipole antenna selectively bonded to a fully swollen PDMS substrate at 2.4 GHz. Fully swollen PDMS was modeled by considering 60% biaxial

strain $(l_2^{Swollen} = 80\ mm, W_2^{Swollen} = 28.8\ m)$ and assigning the measured electrical properties ($K_{Swollen\ PDMS}$ and $Conductivity_{Swollen\ PDMS}$) reported in Table II. Thickness increment in the fully swollen PDMS was theoretically predicted by the Flory–Huggins model [40] which shows 48 μm increase in the PDMS thickness.

2- Mechanics simulation to model the antenna deformation with respect to 0 to 60% strain release in the elastomeric substrate. Strain is: $\varepsilon_x = \Delta l_2/l_2$ and $\varepsilon_y = \Delta W_2/W_2$, where l_2 and W_2 are the length and width of the PDMS support before swelling. Note that, based on the simulation results, 60 % biaxial deformation of the PDMS substrate is the maximum strain level leading to a buckled antenna without the adjacent buckled sections becoming short-circuited. Therefore, 60% swollen PDMS is considered as fully swollen throughout this paper.

3- Electromagnetics simulation of the deformed antenna resulting from step 2 on a relaxed PDMS.

The finite element method was adopted in electromagnetic simulations to calculate return loss values of the antenna. The simulations were performed using COMSOL multiphysics v. 5.3a [41] in which adaptive meshing convergence were used. For efficiency and simplicity, all the metal layers are modeled with transition boundary condition with prescribed thicknesses.

The designed dipole was coupled to the structural mechanics module in COMSOL Multiphysics® software for evaluating the antenna shape after releasing 0-60% biaxial strain due to the PDMS swelling in the presence of chemical vapor (Fig. 2). The degree of PDMS swelling in exposure to diethyl ether was measured experimentally and will be discussed in detail in Section V.

To model the PDMS, a Young's modulus of 549 kPa, a Poisson ratio of 0.5 and mass density of 927 kg/m^3 were used as the materials is considered as a nearly incompressible hyperelastic material [42]. The Yeo model in the nonlinear structural materials module of COMSOL was used to simulate the mechanical behavior of the substrate which can appropriately fit the measured nonlinear stress-strain data of isotropic elastic materials [43]. The strain energy density function for this hyperelasic model is given by:

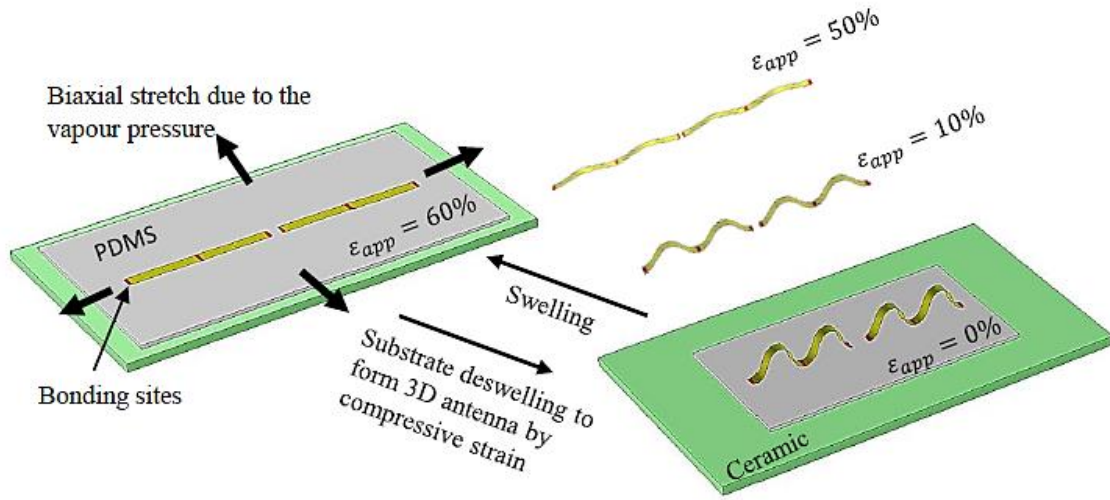$$W = \sum_{i=1}^{3} c_i (I_1 - 3)^i \qquad (1)$$

Fig. 2. Schematic illustration of the designed popup sensor by mechanically guided 3D assembly through PDMS swelling and deswelling.

where W is strain energy density function, I_1 is the first invariant of the Cauchy-Green deformation tensor, c_1, c_2 and c_3 are Yeo material parameters with values of 36.85, 5.81 and 0.97 kPa respectively.

The high permittivity ceramic (commercial name: E-20) is a $MgTiO_3$-$CaTiO_3$ composite provided by T-Ceram [44]. Its function is to reduce the dipole length by dielectric loading and increase the amount of frequency shift after deformation. The simulated antenna was fed with 50 Ω coaxial cable and a perfectly matched layer (PML) was used for the radiation boundary condition. Mesh refinement was adopted to increase the simulation accuracy.

III. EQUIVALENT CIRCUIT MODEL

The popup dipole antenna is a buckled version of its straight counterpart with similarities in terms of radiation pattern and current distribution. In [38] a four element circuit model for a straight dipole antenna was derived which can be adapted to the popup dipole antenna by altering the lumped components values, Fig. 3(a). The proposed circuit model including L_{31}, R_{31}, C_{31} and C_{32} represents the feed-point impedance of a half wavelength dipole and the element values depend only on the physical dimensions of the antenna. To adapt the model, we need to consider the post-buckling behavior of the antenna. As shown in Fig. 2 the buckled structure is formed by compressive buckling of a flat 2D ribbon which is bonded at either end to a strained elastomeric support. Relaxing the strain induces compressive forces which buckle the ribbon into an arc, Fig. 3(c). The compressive strain (ε_{comp}) induced in the antenna is defined as [34]:

$$\varepsilon_{comp} = -\frac{l_{rib}^0 - l_{rib}}{l_{rib}^0} \qquad (2)$$

where l_{rib} is the distance between bonding sites after compression and l_{rib}^0 is the total length of the ribbon

between two bonding sites. The vertical displacements of the ribbon during the buckling were considered in [34]-[36] and the static deflection amplitude of the buckled ribbon (A) is given by [34]:

$$A = \frac{2l_{rib}^0}{\pi} \sqrt{\frac{l_{rib}^0 - l_{rib}}{l_{rib}^0} - \epsilon_c} \qquad (3)$$

where $\varepsilon_c = \pi^2 h^2 / [3(l_{ib}^0)^2]$ is the critical strain for the buckling of the ribbon antenna which is the maximum strain that the antenna can bear while staying flat and h is the ribbon thickness ($30\mu m$). By substituting the post buckling parameters into the equations derived in [38], the value of each lumped element in the equivalent circuit model can be calculated by (4)-(6).

$$C_{31} = \left\{ \frac{12.0674(Nl_{rib})}{\left(\log\left(\frac{2Nl_{rib}}{T}\right) - 0.7245\right)} \right\} \text{ pF} \qquad (4)$$

$$C_{32} = 2Nl_{rib} \left\{ \frac{0.89075}{\left((\log\left(\frac{2Nl_{rib}}{T}\right))^{0.8006} - 0.861\right)} - 0.02541 \right\} \text{ pF} \qquad (5)$$

$$L_{31} = 0.2\, l_1 \left\{ \left(1.4813\, \log\left(\frac{2l_1}{T}\right)\right)^{1.012} - 0.6188 \right\} \mu H \qquad (6)$$

where $l_{rib} = \frac{l_{rib}^0}{(1+\varepsilon_{app})}$, ε_{app} is the strain value in the PDMS, N is the number of bends, $T = \frac{W_1}{4}$, l_1 is the length of each dipole arm and W_l is the width. As the total length of the buckled ribbon has not changed, the self-inductance L_{31} is approximately equal to the self-inductance of a straight dipole. However, buckling introduces mutual capacitances between adjacent ribbon arcs that form a meander section. The mutual capacitance of a meander section is given by:

$$C_m = \frac{\pi K_0 A}{ln\left[\left(\frac{l_{rib}}{T}\right) + \sqrt{\left(\frac{l_{rib}}{T}\right)^2 - 1}\right]} \quad (7)$$

where K_0 is the relative permittivity of free space. The resonant frequency shift can be described in terms of the variation in the antenna capacitance. Therefore, the resonant frequency f_0 of a popup dipole is as follows:

$$f_0 = \frac{1}{2\pi\sqrt{L_{31}(C_{31} + C_{32} + C_m/2N)}} \quad (8)$$

To validate our proposed theoretical model, the predicted resonant frequencies of the dipole antenna with N=2 over 0 to 60% strain in the PDMS substrate are compared with numerical simulations in COMSOL Multiphysics and presented in Fig. 4. The largest deviation in the resonant frequency observed between our model and simulation result was 3.8%.
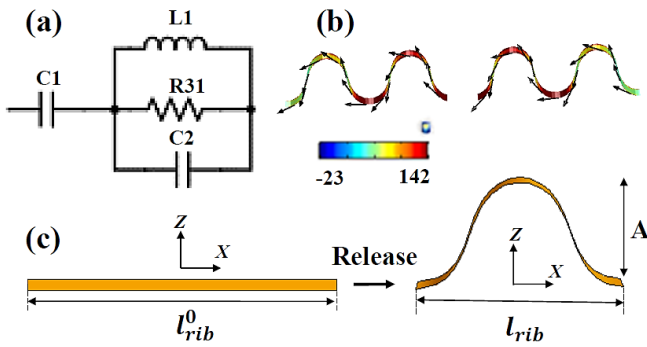

Fig. 3 (a) Equivalent circuit model used for modeling popup dipole antenna [38], (b) Surface current (A/m) on the buckling dipole after deswelling and returning to the original PDMS size, (c) Diagram of mechanics model for a meander section of a buckled ribbon.
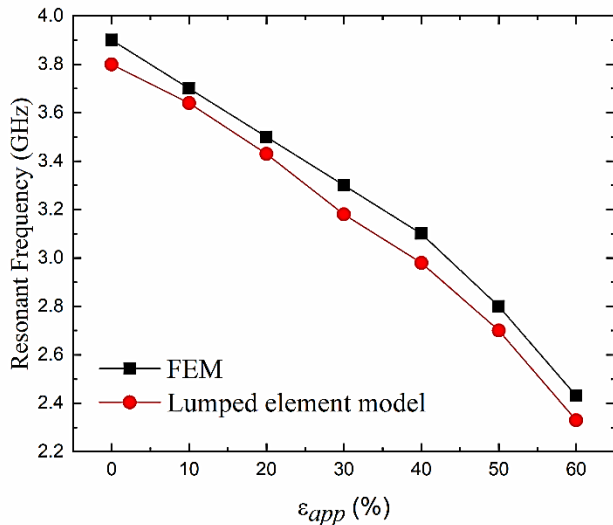

Fig. 4. Resonant frequency as a function of strain value in PDMS (ε_{app}). Plot compares the results from numerical simulation in COMSOL and predictions from geometry-based model. Note that N=2 in this study.

IV. NUMERICAL RESULTS AND DISCUSSION

In order to study the effect of thickness on the antenna input reflection coefficient (S_{11}) and the effect on sensitivity when the sensors are repeatedly stressed and relaxed, three sensor designs with PDSM thicknesses of 0.4, 0.8 and 1mm on a 1mm ceramic substrate are considered. Initially, a dipole was designed for 2.4 GHz on 0.4 mm thick PDMS. The antenna and substrate were placed on a 1 mm thick high-permittivity ceramic substrate to reduce the antenna size. In the next step, the model was coupled to the COMSOL mechanics simulation module to capture all mechanics aspects of 2D to 3D antenna transformation process including strain distribution during compressive buckling after releasing 0 to 60% strain in the PDMS. These amounts of strain are due to the PDMS swelling after exposure to specific concentrations of diethyl ether and will be discussed in Section V. Hollow shell mesh elements were used for the 2D precursor of copper ribbon which is a good conductor with small skin depth meaning the hollow elements will adequately model current flow, while dielectric materials (PDMS and ceramic) require solid elements as E-field penetrates them. The load ramping technique was applied to model the nonlinear buckling process. This method solves a nonlinear problem with gradually increasing load values and using the solutions from each step as the starting value for the next step [45]. As the structure will become unstable when a load reaches its buckling value, applying load in small steps helps for better convergence. By changing the number of bonding sites between dipole and PDMS, the number of buckles (N) in each arm of the dipole can be determined. Fig. 5 presents the Von Mises stress (MPa) in both the antenna (for $N = 2$ and $N = 5$) and PDMS substrate (with 60% strain release). It can be seen that the amount of stress at the bend apexes plus the locations near the bonding sites is higher than all other locations for all dipole configurations. This high amount of cyclic stress could cause damage to the substrate and dipole after a finite number of cycles.
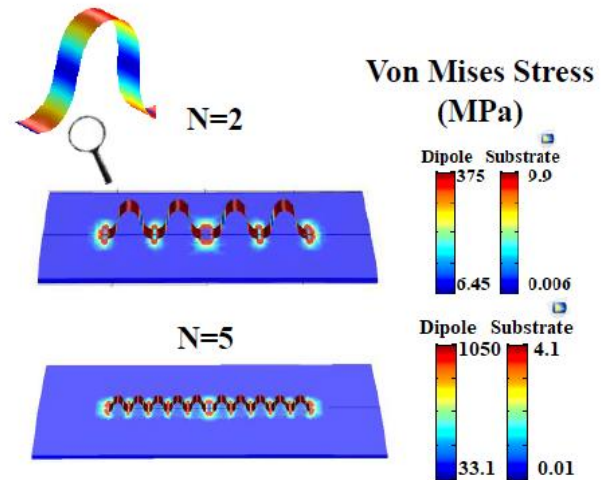

Fig. 5. Von Mises stress (MPa) in the antenna and substrate after release of 60% strain in the PDMS for N=2 & 5.

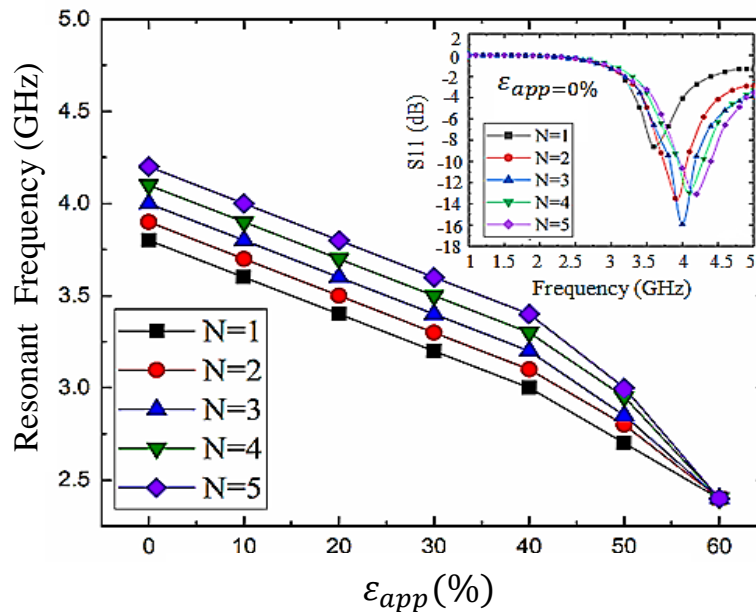Fig. 6. Resonant frequency shift vs strain value in the PDMS substrate for the half wave length dipole antenna with buckled sections $N = 1$ to N=5. Inset figure presents reflection coefficient (dB) versus frequency (GHz) for the sensor in the relaxed mode with unswollen PDMS and shows a good antenna match with N=2 and N=3.

Simulation results show that the maximum level of stress on the dipole significantly increases for higher values of N, and the number of high stress regions increases with N. As the PDMS substrate has a Young's modulus nearly 5 orders of magnitude lower than the metallic ribbon (E_{copper} = 130 GPa), there are high stress levels at the bonding sites.

In the final step, the buckled antenna was again coupled to the RF simulation to determine the amount of resonant frequency shift in the S_{11} plot. When planar, the high permittivity substrate serves to reduce the antenna electrical size. When buckled, the popup structure achieves a reduction in length by expanding the antenna into the third dimension off the substrate. During nonlinear buckling the dipole is bent severely and the number of bends, the height from the PDMS substrate, and finally the distance between neighboring conductors in each arc are crucial factors in determining the amount of resonant frequency shift. The currents flow in opposite directions on adjacent vertical paths and have a cancelling effect, Fig. 3(b), which is stronger when the antenna has multiple bends which are closely packed. In this case, the effective electrical length of the antenna becomes smaller while the physical length remains constant. During compressive buckling, mutual series capacitance arises between the two dipole arms which decreases the overall capacitance. This factor as well as the reduced dielectric loading caused by the separation between the substrate and the bent dipole leads to a resonant frequency up-shift. Fig. 6 shows the simulated resonant frequency (GHz) versus strain values in the PDMS substrate for N values of 1 to 5. The up-shift in the S_{11} graph, confirms that the dipole becomes electrically shorter as expected. The impedance match varies with N=2 or N=3 providing the best match. Although antennas with $N > 2$ show better frequency shift (and better impedance match for $N = 3$), in order to

decide which N value is optimum, the mechanical performance must also be considered. As discussed, cyclic mechanical buckling exerts stress at the antenna–elastomer bonding sites which could lead to eventual failure. Therefore, the mechanical aspects of the design as well as durability should be taken into account and a fatigue study is presented to characterize the optimum N value. Fatigue is a primary cause of damage to structures when subjected to a cyclic loading and can lead to failure at loads below the yield stress limit. The fatigue mechanism consists of crack initiation and crack propagation which leads to progressive and unrecoverable damage. Therefore, the number of cycles required for fatigue crack initiation with the COMSOL Multiphysics fatigue module was studied. A stress-life method using the Wöhler curve approach [46] was applied to predict the number of stress cycles the dipole sustains before failure. Fig. 7 presents the fatigue study results for the buckled dipole where it can be seen that the peaks and the bonding sites are the locations most likely to fail. The possibility of failure at these points is almost a thousand times higher than other locations. The practical values will be somewhat lower in practice because the FEA simulation assumes a perfect bonding of dipole with PDMS substrate without any delamination, while in experiment, all bonds are imperfect. Similarly, by investigating the stress at the bonding locations (Fig. 5) it was realized that with more buckles (N) and thus larger bend angles at the bonding sites the possibility of failure due to the fatigue increases. Therefore, $N = 2$ is considered as an optimum value for the remaining analysis as it provides a good input match with a lower fatigue risk. The same 0 to 60% strain analysis was performed on a 0.8 mm PDMS substrate causing a frequency shift from 3.74 GHz to 2.4 GHz and on a 1 mm thick substrate causing a shift of 3.58 GHz to 2.4 GHz. Fig. 8

shows the return loss (S_{11}) plot for 60% strained and strain-free substrates with different thicknesses of 0.4 mm, 0.8 mm and 1 mm. It can be seen that thinner PDMS provides an improved antenna input match for both the swollen and unswollen modes and the stress simulation results in Table III show the maximum Von Mises stress on the PDMS substrate decreases with increasing thickness.
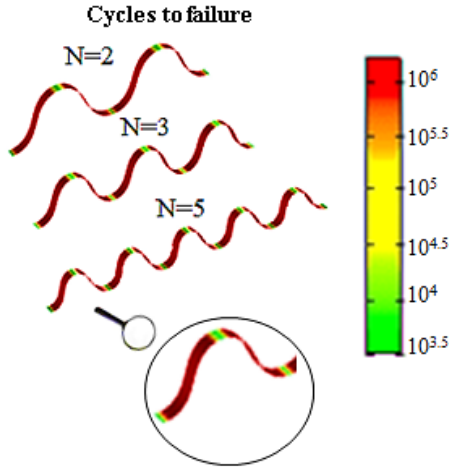

Fig. 7. Number of cycles to failure for the half wavelength dipole antenna on a PDMS substrate after release of 60% strain.

TABLE III
MAXIMUM STRESS LEVEL IN THE PDMS SUBSTRATE WITH DIFFERENT THICKNESSES

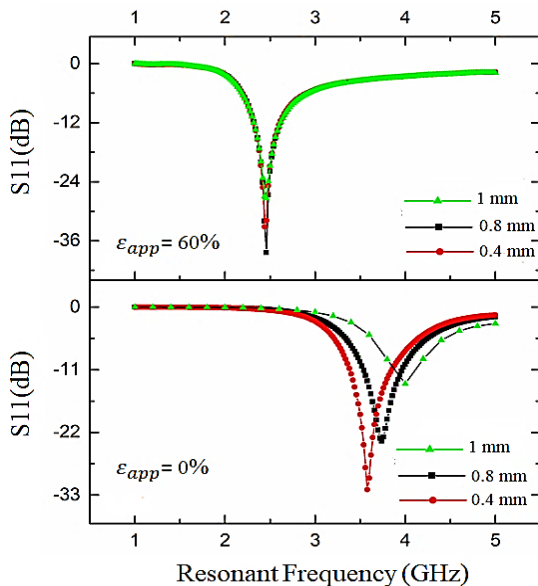| Maximum Von Mises Stress	T_2=0.4 mm	T_2=0.8 mm	T_2=1 mm
MPa	9.9	4.8	4.44

Fig. 8. Return loss (dB) versus frequency (GHz) for half wave dipole on a PDMS substrate with thicknesses of 0.4, 0.8 and 1mm for 60% strained PDMS and strain-free PDMS substrate.

V. EXPERIMENTAL

PDMS pads were cast using the procedure mentioned in [27]. The test environment was a desiccator with an internal diameter of 17 cm, external diameter of 21 cm and internal height of 24 cm. 50 cm^3 of diethyl ether was added to the bottom of the desiccator beneath a perforated disk which supported the PDMS elastomer while allowing exposure to the vapor. Three rectangular PDMS pads with the same width and the length as in Table I but different thicknesses of 0.4 mm, 0.8 mm and 1 mm were placed onto the perforated disk. A flat glass lid was used to seal the desiccator to allow view of the elastomeric substrates. To measure the degree of PDMS swelling with respect to the vapor exposure time, photographs were taken every 30 s. ImageJ software was used to calculate the degree of swelling (biaxial strain percentage) in each photograph. Fig. 9(a) presents the degree of swelling in the three PDMS samples with thicknesses of 0.4 mm, 0.8 mm and 1 mm. From this graph it can be concluded that as the original PDMS thickness is decreased, the swelling response gets faster and thus response time drops. Therefore, 0.4 mm thickness was chosen for the rest of the experiment. For fabricating the sensor, three PDMS substrates of 0.4 mm were placed in the desiccator for 45 min, this led to 60 % swelling in the PDMS. At this point, three flat dipoles with dimensions given in Table I were bonded to each of the fully swollen PDMS substrates with six bonding sites using commercial adhesive (Super Glue, Loctite Company). Then the samples were removed from the desiccator to deswell. Fig. 9(b) presents the fabrication process. When the PDMS/ceramic samples with the antennas were completely deswelled, they were placed into the desiccator above 50 cm^3 diethyl ether and a concave lid with a hole was used to allow connection to a network analyzer (Rohde and Schwarz ZVL 6 GHz) during the gas exposure period. Fig. 9(c) shows the measurement set up. By removing the sensors from the desiccator, the dielectric constant, conductivity and thickness of PDMS layers returned to the pre-exposure values after 25 seconds (for a complete exposure cycle). Therefore the sensor could be utilized multiple times. Each sensor function was experimentally measured twice for a complete cycle of exposure-removal of vapor-exposure to reveal fabrication errors. No noticeable resonant frequency drift occurred throughout the experiments which demonstrated the repeatability of the process. To evaluate the sensitivity, the gas concentration needed to trigger a noticeable shift in the resonant frequency was determined [47]-[49]. Table IV presents the vapor concentration in the desiccator

TABLE IV
SUMMARY OF MEASUREMENT RESULTS

Time (min)	Vapor concentration (ppm)	Degree of swelling (%)	Frequency shift ($\Delta f = f1 - f2$) MHz $f1$=4 GHz
1	36	10	180
6	217	20	440
15	540	30	620
23	828	40	790
35	1260	50	1020
45	1620	60	1520

TABLE V
COMPARISON WITH OTHER WORKS

| Method	Target gas	Response rate (MHz/ppm)	Recovery time(s)	Reference
Carbon Nanotube (CNT) integrated with patch antenna	ammonia (NH_3)	0.4	30	[4]
Graphene Oxide and nano-silver ink loaded on patch antenna	ammonia (NH_3)	0.05	----	[10]
Tin Oxide nanoparticles integrated with patch antenna	ethylene	0.07	----	[12]
Popup dipole antenna integrated with PDMS	diethyl ether	0.6-1.1	25	This work

with respect to the exposure time and the range of resonant frequency shift due to the PDMS swelling. These values are the average performance of three sensor samples with PDMS thickness of 0.4 mm. Measurements in Fig 9(d) show that the minimum detectable vapor concentration is 36 ppm which corresponds to 180 MHz frequency shift and once the sensor is activated, it can detect vapor at the minimum rate of 0.6 MHz/ppm (between low and high concentrations) which is better than the values reported in the recent publications [4], [10], [12], [13]. This rate value is greater (1.1 MHz/ppm) for low vapor concentrations (lower than 300 ppm) which is attributed to the saturation effect in the PDMS substrate. We repeated the same experimental procedure for the solvent acetone. Measurement verified that the swelling degree of the PDMS upon exposure to the acetone vapor is around 63% lower than for diethyl ether. Therefore, by extracting the resonant frequency vs gas concentration graph, our proposed sensor can distinguish between these two vapors. Fig. 9(d) represents the experimental frequency response upon the introduction of various concentration of diethyl ether. It is interesting to note that the response is linear (slope of -6.23e-4) and Fig 9(e) compares the resonant frequency shift with respect to the vapor concentration of diethyl ether and acetone. Linear interpolation was used to obtain the curves. Finally, we compare the proposed gas sensor with previous works in the literature in Table V.

VI. CONCLUSION

The design principle and assembly of a 3D vapor sensor based on compressive buckling is reported. The resonant frequency of the antenna sensor varies with diethyl ether concentration which is attributed to the stretch and compression of the antenna through swelling/deswelling of the PDMS support. Our proposed sensor has the advantage of improved sensitivity, simple fabrication and low cost compared to reported alternatives, which makes it a good candidate for cost-effective environmental monitoring for places such as laboratories and hospitals. Repeatability of the sensor performance was verified by both fatigue study (simulation) and experiment through measuring the outputs of three sensor prototypes and repeating each experiment twice. Future research will focus on wireless remote reading

(a)

(b)
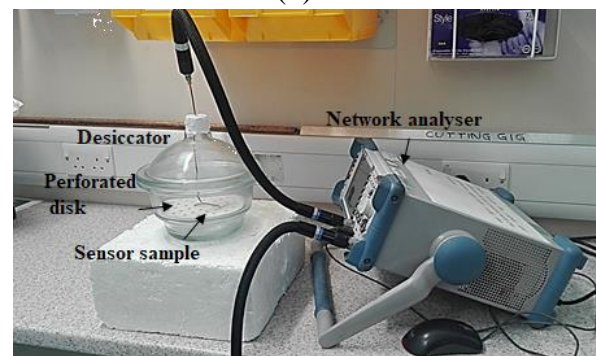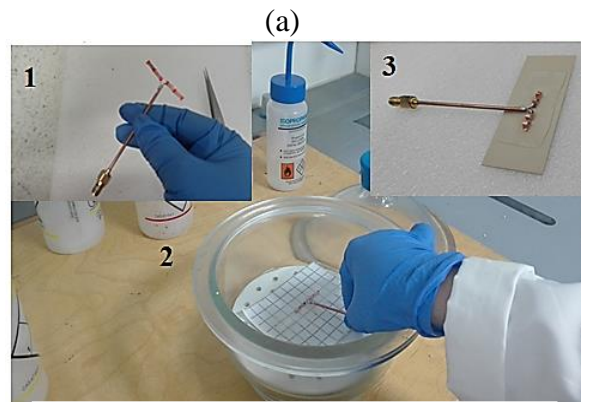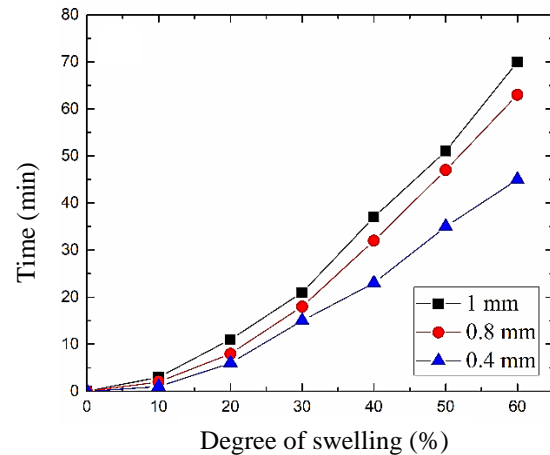
(c)
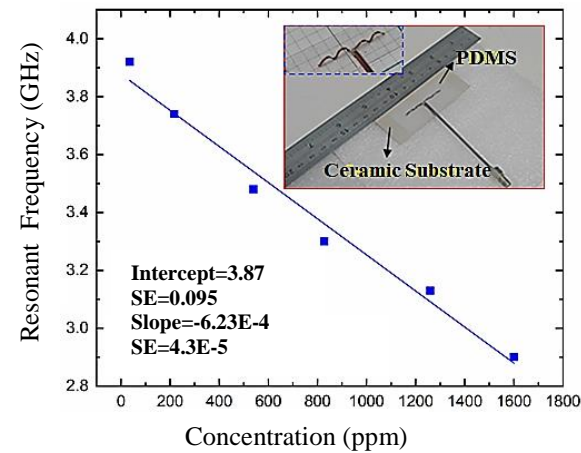
(d)
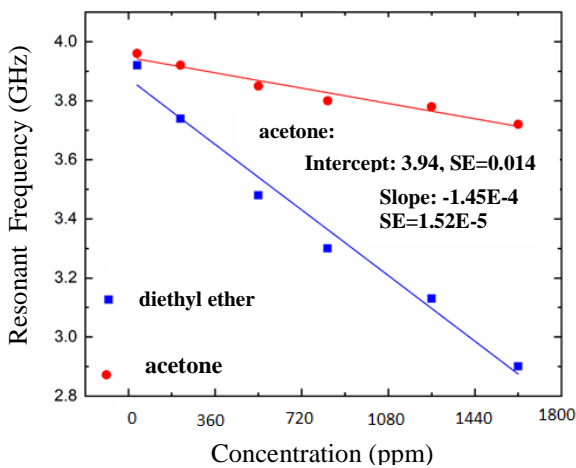
(e)

Fig. 9 (a) Swelling degree vs exposure time for three thicknesses (0.4 mm, 0.8 mm and 1 mm), (b) Fabrication process. Step one, the flat dipole antenna is superglued at six bonding zones (specified with red color). In step two, the antenna is attached to the fully swollen PDMS in the desiccator. Note that all experiments were performed in clean room to ensure the safety and finally in step three, the sample is removed from the desiccator to deswell. At this point due to the induced compressive force, buckled dipole is formed., (c) Experimental set up, sensor placement in desiccator, (d) Experimental curve for resonant frequency vs diethyl ether concentration (ppm), Linear correlation between frequency and gas concentration could be used for calibrating the sensor. (e) A comparison of resonant frequency vs gas concentration curve between diethyl ether and acetone.

of the sensor using radar or link coupling techniques.

VII. ACKNOWLEDGEMENTS

VIII. REFERENCES

[1] H. S. Sing, "an effective approach for the detection of explosives", *J. Hazard. Mater*, vol. 144, pp. 15-28, Feb, 2007.

[2] *Hazardous Substance Fact Sheet | New Jersey Department of Health and Senior Services*, 1996. [Online]. Available: https://nj.gov/health/eoh/rtkweb/documents/fs/0701.pdf, [Accessed: April-2002].

[3] *Product Safety Summary Sheet | DuPont^{TM}*, 2012. [Online], Available: http://www2.dupont.com/inclusive-innovations/en-us/sites/default/files/Dimethyl%20Ether%20Product%20Safety%20Summary.pdf. [Accessed: 25- September-2012].

[4] H. Lee *et al*., "Carbon-Nanotube Loaded Antenna-Based Ammonia Gas Sensor," in *IEEE Transactions on Microwave Theory and Techniques*, vol. 59, no. 10, pp. 2665-2673, Oct. 2011.

[5] K. G. Ong, K. Zeng and C. A. Grimes, "A wireless, passive carbon nanotube-based gas sensor," in *IEEE Sensors Journal*, vol. 2, no. 2, pp. 82-88, April 2002.

[6] C. Occhiuzzi, A. Rida, G. Marrocco "RFID Passive Gas Sensor Integrating Carbon Nanotubes," in *IEEE Transactions on Microwave Theory and Techniques*, vol. 59, no. 10, pp. 2674-2684, Oct. 2011.

[7] H. Lee, K. Naishadham, M. M. Tentzeris and G. Shaker, "A novel highly-sensitive antenna-based "smart skin" gas sensor utilizing carbon nanotubes and inkjet printing," *2011 IEEE International Symposium on Antennas and Propagation (APSURSI)*, WA, 2011, pp. 1593-1596.

[8] M. M. Tentzeris and S. Nikolaou, "RFID-enabled ultrasensitive wireless sensors utilizing inkjet-printed antennas and carbon nanotubes for gas detection applications," *2009 IEEE International Conference on Microwaves, Communications, Antennas and Electronics Systems*, Tel Aviv, 2009, pp. 1-5.

[9] K. Na, H. Ma, J. Park, J. Yeo, J. Park and F. Bien, "Graphene-Based Wireless Environmental Gas Sensor on PET Substrate," in *IEEE Sensors Journal*, vol. 16, no. 12, pp. 5003-5009, June15, 2016.

[10] B. Wu, X. Zhang, B. Huang *et al.,* " High-Performance Wireless Ammonia Gas Sensors Based on Reduced Graphene Oxide and Nano-Silver Ink Hybrid Material Loaded on a Patch Antenna", in *sensors,* vol. 17, no. 9, pp. 2070-2081, Sep. 2017.

[11] A. Quddious, S. Yang, M. M. Khan *et al.,* " Disposable, paper-based, inkjet-printed humidity and H2S gas sensor for passive sensing applications", in *sensors*, vol. 16, no. 12, pp. 2073-2086, Dec. 2016.

[12] M. D. Balachandran, S. Shrestha, M. Agarwal, Y. Lvov and K. Varahramyan, "SnO2 capacitive sensor integrated with microstrip patch antenna for passive wireless detection of ethylene gas," in *Electronics Letters*, vol. 44, no. 7, pp. 464-466, 27 March 2008.

[13] M. H. Zarifi, A. Sohrabi, P. M. Shaibani, M. Daneshmand and T. Thundat, "Detection of Volatile Organic Compounds Using Microwave Sensors," in *IEEE Sensors Journal*, vol. 15, no. 1, pp. 248-254, Jan. 2015.

[14] H. Guo, L. Lou, X. Chen and C. Lee, "PDMS-Coated Piezoresistive NEMS Diaphragm for Chloroform Vapor Detection," in *IEEE Electron Device Letters*, vol. 33, no. 7, pp. 1078-1080, July 2012.

[15] A. Sohrabi, P. Mojir Shaibani, M. H. Zarifi, M. Daneshmand and T. Thundat, "A novel technique for rapid vapor detection using swelling polymer covered microstrip ring resonator,"*2014 IEEE MTT-S International Microwave Symposium)*, Tampa, FL, 2014, pp. 1-4.

[16] X. Ning, J. Yang, C. L. Zhao, and C. C. Chan, "PDMS-coated fiber volatile organic compounds sensors," Appl. Opt. vol. 55, no. 13, pp. 3543-3548, 2016.

[17] N. Gao, X. Zhang, S. Liao, H. Jia, and Y. Wang, "Contribution of polymeric swelling to the overall response of capacitive gas sensors", in *Anal. Bioanal. Chem*., vol. 405, pp. 6445-6452, May. 2013.

[18] M. D. Balachandran, S. Shrestha, M. Agarwal, Y. Lvov, "Polymer Swelling Induced Conductive Wrinkles for an Ultrasensitive Pressure Sensor", in *ACS Macro Lett*., vol. 5, no. 7, pp. 823-827, June 2016.

[19] S. H. Jeong, S. Zhang, K. Hjort, J. Hilborn, Z. Wu, "PDMS-Based Elastomer Tuned Soft, Stretchable, and Sticky for Epidermal Electronics ", in *Advanced Materials,* vol. 28, no. 28, pp. 5830-5836, July. 2016.

[20] C. M. Hipatl, S. M. Aguirre, G. B. Perez, *et al*. "Detection of volatile organic compounds by an interferometric sensor", in *Sens. Actuator*, B, vol. 147, no. 1, pp. 37-42, May. 2010.

[21] H. K. chang, G. T. Chang, A. K. Thokchom, *et al*. "Ultra-fast responsive colloidal–polymer composite-based volatile organic compounds (VOC) sensor using nanoscale easy tear process", in *Sci Rep*, vol. 8, no. 5291, March 2018.

[22] N. Tiercelin, F. Coquet, R. Sauleau, *et al*. "Polydimethylsiloxane membranes for millimeter-wave planar ultra-flexible antennas", *in J Micromech Microeng,* vol. 16, pp. 2389-2395, July, 2006.

[23] Q.Y. Tang, Y. M. Pan, Y.C.Chan, K.W.Leung, "Frequency-tunable soft composite antennas for wireless sensing", in *Sens. Actuator, A,* vol. 179, pp. 137-145, June. 2012.

[24] H. Kou, L. Zhang. Q. Tan, et al. "Wireless flexible pressure sensor based on micro-patterned Graphene/PDMS composite", in *Sens. Actuator, A,* vol. 277, pp. 150-156, July. 2018.

[25] A. Nag *et al.*, "A Transparent Strain Sensor Based on PDMS-Embedded Conductive Fabric for Wearable Sensing Applications," in *IEEE Access*, vol. 6, pp. 71020-71027, 2018.

[26] M. Liu, J. Sun, Y. Sun, C. Bock and Q. Chen, "Thickness-dependent mechanical properties of polydimethylsiloxane membranes", in *J Micromech Microeng,* vol. 19, no. 3, pp. 035028–035031, Jan. 2009.

[27] C. V. Rumens , M. A. Ziai , K. E. Belsey , J. C. Batchelor, S. J. Holder, "Swelling of PDMS networks in solvent vapours; applications for passive RFID wireless sensors", *J. Mater. Chem. C*, vol. 3, pp. 10091-10098, Aug, 2015.

[28] K. E. Belsey, A. V. S. Parry, C. V. Rumens, M. A. Ziai, S. G. Yeates , J. C. Batchelor, S. J. Holder, 'Switchable disposable passive RFID vapour sensors from inkjet printed electronic components integrated with PDMS as a stimulus responsive material ", *J. Mater. Chem. C*, vol. 5, no. 12, pp. 3167-3175, Jan, 2017.

[29] S. Xu, Z. Yan, K. I. Jang, W. Huang, H. Fu, J. Kim, *et al.* "Assembly of micro/nanomaterials into complex, three dimensional architectures by compressive buckling", *Science*, vol. 347, pp. 154-159, 2015.

[30] Y. Zhang, Z. Yan, K. Nan, *et al.* "A mechanically driven form of Kirigami as a route to 3D mesostructures in micro/nanomembranes", in *PNAS USA,* vol. 112, no. 38, pp. 11757-11764, Sep. 2015.

[31] li. Gao, Y. Zhang, H. Zhang, *et al*. "Optics and Nonlinear Buckling Mechanics in Large-Area, Highly Stretchable Arrays of Plasmonic Nanostructures", in *ACS Nano,* vol. 9, no. 6, pp. 5968–5975, Apr. 2015.

[32] Z. Yan, F. Zhang, J. Wang, *et al*. "Controlled Mechanical Buckling for Origami-Inspired Construction of 3D Microstructures in Advanced Materials ", in *Adv. Funct. Mater,* vol. 26, no. 16, pp. 2629-2639, Feb. 2016.

[33] R. Li, M. Li Y. Su, *et al*. "An analytical mechanics model for the island-bridge structure of stretchable electronics ", in *Soft Matter*, vol. 9, no. 35, pp. 8476-8482, Jul. 2013.

[34] W. Heling, N. Xin, L. Haibo, *et al.* "Vibration of mechanically-assembled 3D microstructures formed by compressive buckling ", in *J Mech Phys Solids,* vol. 12, pp. 187-208, Mar. 2018.

[35] S. Li, M. Han, J. A. Rogers, *et al*. "Mechanics of buckled serpentine structures formed via mechanics-guided, deterministic three-dimensional assembly "in *J Mech Phys Solids,* vol. 125, pp. 736-748, Apr. 2019.

[36] B. Wang, S. Bao, S. Vinnikova, et al. "Buckling analysis in stretchable electronics", in *npj Flex. Electron.* vol. 1, no. 5, Oct. 2017.

[37] *Dak 3.5 | SPEAG.* Accessed: June 06, 2018. [Online]. Available:https://www.speag.com/products/dak/dak-dielectric-probe-systems/dak-3-5-200-mhz-20-ghz.

[38] T. G. Tang, Q. M. Tieng and M. W. Guun, "Equivalent circuit of a dipole antenna using frequency-independent limped elements", in IEEE Trans. Antennas Propag, vol. 41, no. 1, pp. 100-103, Jan. 1993.

[39] O. O. Olaode, W. D. Palmer and W. T. Joines, "Characterization of Meander Dipole Antennas with a Geometry-Based, Frequency-Independent Lumped Element Model," in *IEEE Antennas and Wireless Propagation Letters*, vol. 11, pp. 346-349, Mar. 2012.

[40] W. Mönch, J. Dehnert, E. Jaufmann, and H. Zappe, "Flory–Huggins swelling of polymer Bragg mirrors," *Appl. Phys. Lett.*, vol. 89, no. 16, p. 164104, 2006.

[41] Structural mechanics, RF, Nonlinear structural materials and Fatigue modules, COMSOL multiphysics v. 5.3 a, www.comsol.com, COMSOL AB, Stockholm, Sweden.

[42] D. Armani, C. Liu and N. Aluru, "Re-configurable fluid circuits by PDMS elastomer micromachining," *Technical Digest. IEEE International MEMS 99 Conference. Twelfth IEEE International Conference on Micro Electro Mechanical Systems (Cat. No.99CH36291)*, Orlando, FL, USA, pp. 222-227. Jan. 1999.

[43] P. A. L. S. Martins, R. M. N. Jorge, A. J.M. Ferreira, "A Comparative Study of Several Material Models for Prediction of Hyperelastic Properties: Application to Silicone-Rubber and Soft Tissues ", in *Strain*, vol. 42, pp. 135-147, Jul 2006.

[44] T-Ceram RF and Microwave Company, Website: http://www.t-ceram.com.

[45] W. Frei, "Load Ramping of Nonlinear Problems," *Comsol Blog*, Nov 2013. https://uk.comsol.com/blogs/load-ramping-nonlinear-problems/

[46] W. Schutz "A history of fatigue ", *in Eng Fract Mech*, vol. 54, no. 2, pp. 263-300, May 1996.

[47] M. Abdolrazzaghi, M. Daneshmand and A. K. Iyer, "Strongly Enhanced Sensitivity in Planar Microwave Sensors Based on Metamaterial Coupling," in *IEEE Transactions on Microwave Theory and Techniques*, vol. 66, no. 4, pp. 1843-1855, April 2018.

[48] M. Abdolrazzaghi, M. Daneshmand, "Sensitivity Optimization in SRRs Using Interferometry Phase Cancellation,'' in *2019 IEEE MTT-S International Microwave Symposium (IMS),* Boston, MA, USA, 2019, pp. 1495-1498.

[49] M. Abdolrazzaghi, N. Kazemi and M. Daneshmand, "Sensitive Spectroscopy Using DSRR Array and Linvill Negative Impedance," in *2019 IEEE MTT-S International Microwave Symposium (IMS)*, Boston, MA, USA, 2019, pp. 1080-1083.

Shaghayegh Soltani (S'18) received the B.Sc. and M.Sc. degrees in Electrical engineering (Telecommunications) from the University of Shahid Beheshti, Tehran, Iran in 2013 and Khajeh Nasir Toosi University of Technology, Tehran, Iran, in 2016, respectively. She is currently pursuing the Ph.D. degree with the Communication Research Group, University of Kent, Canterbury, UK. Her current research interests include antenna modelling for UHF Radio Frequency Identification (RFID) tags and skin-mountable sensors.

Aaron J. R. Hillier received the M.Sc. degree in forensic science from the University of Kent, Canterbury, U.K., in 2015, where he is currently pursuing the Ph.D. degree with the Communication Research Group and the Functional Materials Group. His current research interests include stimuli responsive polymers, passive sensing, and bodycentric antennas.

Simon Holder researched for his PhD in organic Chemistry at the University of Hull under Dr David Lacey, as part of the Liquid Crystal Group. He received his PhD in 1993 and went on to work as a postdoctoral research fellow at the University of Kent on polysilane materials with Professor Dick Jones and subsequently on supramolecular materials at the University of Nijmegen with Professor Roeland Nolte. He was appointed as a Lecturer in Organic Chemistry at Kent in 1999 and a Reader in Organic Chemistry in 2013. Current research projects include the development of materials for RFID sensors, novel polymer super-absorbents and self-assembling block copolymers.

John C. Batchelor (S'93–M'95–SM'07) received the B.Sc. and Ph.D. degrees from the University of Kent, Canterbury, U.K., in 1991 and 1995, respectively. From 1994 to 1996, he was a Research Assistant with the Electronics Department, University of Kent, where he became a Lecturer of electronic engineering in 1997. He is currently the Leader of the Antennas Group at the University of Kent and the Professor of antenna technology. His current research interests include UHF RFID tag design, passive sensing, body-centric antennas, printed antennas, compact multiband antennas, electromagnetic bandgap structures, and long-wavelength frequency selective surfaces.